

TOURMALINE-BEARING QUARTZ VEINS IN THE BARABOO QUARTZITE, WISCONSIN: OCCURRENCE AND SIGNIFICANCE OF FOITITE AND “OXY-FOITITE”

L. GORDON MEDARIS JR.[§] AND JOHN H. FOURNELLE

*Department of Geology and Geophysics, University of Wisconsin-Madison,
Madison, Wisconsin 53706, U.S.A.*

DARRELL J. HENRY

*Department of Geology and Geophysics, Louisiana State University,
Baton Rouge, Louisiana 70808, U.S.A.*

ABSTRACT

The alkali-deficient tourmaline, foitite $[\square(\text{Fe}^{2+}_2\text{Al})\text{Al}_6\text{Si}_6\text{O}_{18}(\text{BO}_3)_3(\text{OH})_3(\text{OH})]$, and associated hematite occur in quartz veins that cut the geon 17 Baraboo Quartzite in south-central Wisconsin. The bluish green prismatic crystals of tourmaline are chemically zoned from core to rim, with the cores being very aluminous, highly alkali-deficient and, in one sample, relatively magnesian. Electron-microprobe analyses demonstrate that the tourmaline has a prevailing alkali-deficiency in the X site, which ranges from 49 to 87%, with a mean of 73%, making this the most alkali-deficient tourmaline reported to date. In one sample, high contents of Al (up to 7.7 Al *apfu*) and high cation-charge excess demonstrate the likely existence of a dominant “oxy-foitite” component $[\square(\text{Fe}^{2+}\text{Al}_2)\text{Al}_6\text{Si}_6\text{O}_{18}(\text{BO}_3)_3(\text{OH})_3(\text{O})]$, which is the first recognition of such in a natural occurrence. The wide range of chemical zoning in the tourmaline is most consistent with substitutions represented by the $\square\text{Al}(\text{NaR})_{-1}$, $\text{AlO}[\text{R}(\text{OH})]_{-1}$, FeAl_{-1} and MgFe_{-1} exchanges, where R symbolizes Fe + Mg. The alkali-deficient character of the Baraboo tourmaline largely reflects the alkali-depleted and chemically mature composition of the host Baraboo Quartzite, but core-to-rim compositional variation in the tourmaline records the evolving nature of the attendant hydrothermal fluid, from a Na-poor, relatively alkaline early stage to a more sodic, acidic later stage.

Keywords: foitite, “oxy-foitite”, Baraboo Quartzite, Wisconsin, U.S.A.

SOMMAIRE

On trouve la foitite $[\square(\text{Fe}^{2+}_2\text{Al})\text{Al}_6\text{Si}_6\text{O}_{18}(\text{BO}_3)_3(\text{OH})_3(\text{OH})]$, pôle du groupe de la tourmaline déficitaire en alcalins, en association avec l'hématite dans des veines de quartz recoupant la quartzite de Baraboo (géon 17) dans le centre-sud du Wisconsin. Les cristaux vert bleuâtre prismatiques de tourmaline sont zonés du coeur vers la bordure; le coeur est fortement alumineux, déficitaire en alcalins et, dans un échantillon, magnésien. Les analyses à la microsonde électronique montrent que la tourmaline accuse un déficit important au site X, entre 49 et 87%, en moyenne 73%, faisant de ce groupe de compositions le plus déficitaire en alcalins qui soit. Dans un échantillon, les teneurs élevées en Al (jusqu'à 7.7 Al atomes par unité formulaire) et l'excédent en charges positives démontrent l'existence probable d'une composante “oxy-foitite” $[\square(\text{Fe}^{2+}\text{Al}_2)\text{Al}_6\text{Si}_6\text{O}_{18}(\text{BO}_3)_3(\text{OH})_3(\text{O})]$, ce qui est en fait le premier exemple à être signalé dans la nature. On interprète l'étendue de la zonation chimique dans la tourmaline en termes de substitutions représentées par les échanges $\square\text{Al}(\text{NaR})_{-1}$, $\text{AlO}[\text{R}(\text{OH})]_{-1}$, FeAl_{-1} et MgFe_{-1} ; ici, R représente Fe + Mg. Le déficit en alcalins de la tourmaline de Baraboo témoigne surtout du déficit en alcalins et le caractère chimiquement mature de l'hôte, la quartzite de Baraboo. La zonation des cristaux résulterait de l'évolution du système hydrothermal, au départ à faible teneur en Na et relativement alcalin, et vers la fin plus sodique et plus acide.

(Traduit par la Rédaction)

Mots-clés: foitite, “oxy-foitite”, quartzite de Baraboo, Wisconsin, Etats-Unis.

[§] E-mail address: medaris@geology.wisc.edu

INTRODUCTION

Alkali-deficient tourmaline, in which the *X* site is incompletely filled by Na or Ca, occurs in alkali-poor and aluminum-rich geological settings, in rocks that have interacted with hydrothermal fluids. The geological settings include certain types of granitic pegmatites (Pezzotta *et al.* 1996, Aurisicchio *et al.* 1999, Selway *et al.* 1999, Dutrow & Henry 2000, Novák & Taylor 2000, Selway *et al.* 2000), hydrothermally altered volcanic and sedimentary rocks (Foit *et al.* 1989, Jiang *et al.* 1997, Hawthorne *et al.* 1999, Pesquera *et al.* 1999), hydrothermal quartz veins (Francis *et al.* 1999, Yavuz *et al.* 1999, Henry *et al.* 2002), and metakarstbauxite (Henry & Dutrow 2001). In these occurrences, three species of alkali-deficient tourmaline are important: foitite, magnesiofoitite, and “oxy-foitite” (Table 1). Foitite, which was formally described and named by MacDonald *et al.* in 1993, is the alkali-deficient analogue of schorl, the common tourmaline. A magnesian counterpart, magnesiofoitite, which was recognized by Hawthorne *et al.* in 1999, is the alkali-deficient analogue of dravite. There is also a theoretical *X*-site-vacant deprotonated end-member of the tourmaline group, “oxy-foitite”, which has been proposed by Hawthorne & Henry (1999).

During a comprehensive investigation of Proterozoic rocks in the Baraboo Range, Wisconsin, it was determined that highly alkali-deficient tourmaline is the characteristic tourmaline in quartz veins in the Baraboo Quartzite (Medaris & Fournelle 2000). Because of the relative chemical simplicity of the quartz veins, constituent tourmaline, and surrounding quartzite, it is feasible to evaluate the nature and range of substitutions that control *X*-site vacancies in tourmaline, to assess the possible existence of “oxy-foitite” in a natural setting, and to infer the nature of fluids associated with quartz veins in the Baraboo Quartzite.

OCCURRENCE

The geon-17 Baraboo Quartzite is a 1500-meter-thick sequence of supermature quartz arenite and sub-

ordinate siltstone and mudstone, which was transformed to quartzite, argillite, and phyllonite during 1.63 Ga low-grade metamorphism (Medaris *et al.* 2003). The Baraboo metasedimentary rocks, which are composed essentially of SiO₂, TiO₂, Al₂O₃, Fe₂O₃, and H₂O, have a Chemical Index of Alteration (CIA) that ranges from 96.8 to 98.8, ranking them among the most chemically mature sedimentary rocks in the geological record [CIA is defined as 100*molar Al₂O₃/(Al₂O₃ + K₂O + Na₂O + CaO)]. Such a mature chemical composition is reflected in the mineralogical composition of the metasedimentary rocks, which consist predominantly of quartz and pyrophyllite, accompanied by accessory hematite and rutile.

Quartz veins, which likely originated during the 1.63 Ga metamorphism and deformation, are relatively abundant and widely distributed in the Baraboo Quartzite. The quartz veins are composed almost entirely of quartz, except for local concentrations of tourmaline and specular hematite. In addition, quartz veins that cut a paleosol at the base of the Baraboo Quartzite contain muscovite, which was introduced after formation of the quartz veins by regionally extensive, but stratigraphically restricted, migration of brine at 1.45 Ga (Medaris *et al.* 2003). Three samples of tourmaline-bearing quartz veins from low in the Baraboo stratigraphic section were selected for investigation: Sample 1 is a folded, 1.5-cm-thick quartz vein in the regolith of the paleosol underlying the quartzite in Baxter Hollow (NW¼, Sec33, T11N, R6E), Sample 2 is a 3-cm-thick quartz vein in quartzite in Baxter Hollow (SE¼, Sec29, T11N, R6E), and Sample 3 is a 3-mm-thick, tourmaline-rich quartz vein that cuts quartzite and metapelite in Pine Hollow (NW¼, Sec35, T11N, R6E).

The three samples analyzed are mineralogically simple, consisting of quartz, specular hematite, and tourmaline, which typically occurs in clusters of small (<1 mm), randomly oriented, prismatic crystals (Fig. 1). The tourmaline is strongly pleochroic, with *O* medium bluish green and *E* almost colorless. Tourmaline in Sample 3 is optically zoned, such that grain rims have a darker color than the cores.

IMAGING AND ANALYTICAL PROCEDURES

Imaging

The character of chemical zoning in the Baraboo tourmaline was revealed by back-scattered electron (BSE) images and element-distribution maps. Because compositional zoning in different samples involves distinct patterns of variation among the light elements, Na, Mg, and Al, BSE images alone are insufficient to portray the precise nature of zoning, and element-distribution maps are required. BSE images and element-distribution maps were acquired at 15 keV with 30 nA beam (Faraday cup) current. Element-distribution maps were acquired at 2000× magnification, 0.05 s dwell time per

TABLE 1. TOURMALINE SPECIES OF SIGNIFICANCE IN THE BARABOO QUARTZ VEINS

Species	(X)	(Y ₃)	(Z ₆)	T ₆ O ₁₈	(BO ₃) ₃	(Y) ₃	(W)
Schorl	Na	Fe ²⁺ ₃	Al ₆	Si ₆ O ₁₈	(BO ₃) ₃	(OH) ₃	(OH)
Dravite	Na	Mg ₃	Al ₆	Si ₆ O ₁₈	(BO ₃) ₃	(OH) ₃	(OH)
Foitite*	□**	Fe ²⁺ ₃ Al	Al ₆	Si ₆ O ₁₈	(BO ₃) ₃	(OH) ₃	(OH)
Magnesiofoitite	□	Mg ₂ Al	Al ₆	Si ₆ O ₁₈	(BO ₃) ₃	(OH) ₃	(OH)
“Oxy-foitite”***	□	Fe ²⁺ Al ₂	Al ₆	Si ₆ O ₁₈	(BO ₃) ₃	(OH) ₃	(O)

* End-member formula modified from the initial formula (Hawthorne & Henry 1999)

** X-site vacancy

*** Hypothetical species of tourmaline not currently approved by the CNMNM, IMA.

pixel, and 2 $\mu\text{m}/\text{pixel}$ spacing. We utilized a combination of WDS and EDS channels, and employed WinEDS hardware/software for acquisition of the energy-dispersion spectra (EDS) and MicroImage software to produce mosaics for the element-distribution maps.

Electron-microprobe (EMP) analysis and normalization procedures

Tourmaline was analyzed by wavelength-dispersion spectrometry (WDS) with a Cameca SX51 instrument, using a 15 kV accelerating voltage, a 10 nA beam (Faraday cup) current, a beam diameter of 1 μm , Probe for Windows software utilizing the matrix correction of Armstrong (1988), and a combination of natural and synthetic minerals as standards.

Analysis of tourmaline by electron microprobe (EMP) presents a challenge because of the inability to measure amounts of Li and H directly, the difficulty in determining amounts of B and O precisely, and the uncertainty in the valence of transition elements. We assumed that Li contents are minimal in the Baraboo tourmaline because of the paucity of other elements of Group Ia, as well as Group IIa, in the geochemical environment of the quartz veins. The preferred method for calculating cation proportions in Li-poor tourmaline is to normalize the sum of $T + Z + Y$ cations to 15, assuming no vacancies (or deficiencies) in the T , Z , or Y sites (Henry & Dutrow 1996). Such a normalization procedure is effective because knowledge of B concentration, OH content, and oxidation state of Fe is unnecessary, and it allows an approximation of OH and oxidation state to be made, based on charge balance. The amount of B_2O_3 necessary to produce three B cations in the structural formula was calculated from stoichiometric constraints, because we do not expect ^{14}B in these Fe-rich tourmaline samples. Fe is reported as Fe^{2+} in the representative EMP analyses (Table 2), but we recognize that tourmaline from these hematite-bearing samples may contain significant amounts of Fe^{3+} . This possibility is examined further below. Finally, O^{2-} substitution for OH^- (deprotonation), calculated by charge balance, is assigned to the W site, owing to preferential incorporation of O^{2-} at the W site relative to the V site (Henry & Dutrow 1996, Hawthorne & Henry 1999).

RESULTS

BSE images and element-distribution maps

BSE images and element-distribution maps reveal the existence of discrete cores and rims of grains, as best illustrated in Samples 2 and 3 (Figs. 2, 3). The euhedral morphology of the core relative to the rim observed in the BSE image implies that the rim is an overgrowth on the precursor tourmaline core, rather than a replacement of that tourmaline (*cf.* Henry *et al.* 2002). However, the chemical variations that are responsible for the BSE

zoning are better revealed by EMP spot analyses (below) and element-distribution maps (Fig. 3). Sample 2 is different from samples 1 and 3 in that it contains Mg-

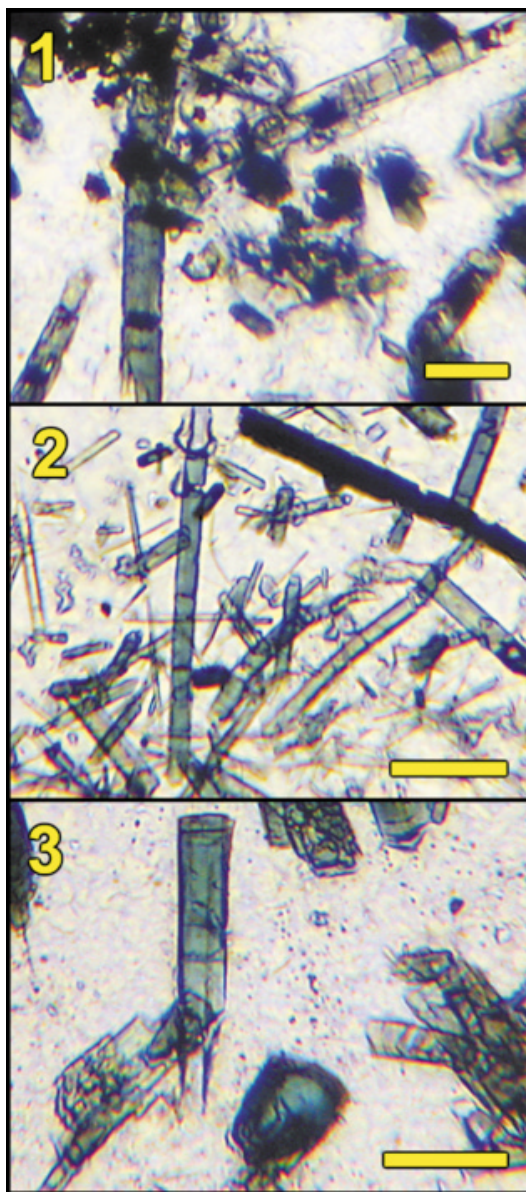


FIG. 1. Photomicrographs of foitite in samples 1 (upper), 2 (middle), and 3 (lower) from quartz veins in the Baraboo Quartzite (plane-polarized light). Scale bars are 50 μm in each panel. Matrix material is quartz, and opaque grains are hematite. Note the optical zoning in tourmaline of sample 3 (the grain cut is approximately perpendicular to the c axis).

rich, Na-poor cores surrounded by Fe-rich, Na-rich rims, with Na decreasing at the outer rims. Sample 1 (not shown) and Sample 3 have Al-rich, Na-poor cores surrounded by Fe-rich, Na-rich rims.

Tourmaline composition and chemical zoning characteristics

The chemical composition of the Baraboo tourmaline reflects the chemical simplicity of the host quartz veins and surrounding quartzite. The tourmaline was analyzed for Si, Ti, Al, Fe, Mn, Mg, Ca, Na, K, F and Cl, but only Si, Al, Fe, Mg and Na were detected (Table 2). In all three samples, the *T* site of tourmaline is fully occupied by Si (6.02 ± 0.05 , 6.07 ± 0.05 , and 6.01 ± 0.04 atoms per formula unit [*apfu*]). The tourmaline is aluminous, with total Al ranging widely from 6.39 to 7.74 *apfu*. In terms of Fe and Mg contents, samples 1 and 3 are Fe-rich, with Fe/(Fe + Mg) values of 0.929 ± 0.01 and 0.999 ± 0.01 , respectively. Sample 2 has a wider range of Fe/(Fe + Mg), with a mean of 0.761 ± 0.16 . The fundamental alkali-deficient nature of the Baraboo tourmaline is demonstrated by less than 50%

occupancy of the *X* site by Na in each sample, with mean occupancies being 0.31 ± 0.09 , 0.25 ± 0.05 , and 0.25 ± 0.08 *apfu*. Consequently, this tourmaline can be generally classed as a vacancy-group tourmaline (Hawthorne & Henry 1999). However, the specific classification and details of the controlling substitutions are best revealed by plotting results of individual EMP analyses on a series of compositional diagrams (Figs. 4–7).

Because all of the analyzed grains of tourmaline are aluminous (Al > 6 *apfu*), the optimal diagram for classification of the tourmaline species is one in which *X* vacancy/(Na + *X* vacancy) is plotted versus Fe/(Fe + Mg) (Fig. 4A). This diagram does not specifically take into account the *W*-site anion occupancy, and each of the fields may also represent fluor- or oxy-equivalents of the tourmaline species. However, F contents are below detection levels for all samples and, as noted below, *W*-site O²⁻ contents are only dominant in the core of Sample 3 tourmaline. Consequently, the foitite field in Figure 4A could also be considered an “oxy-foitite” field for those “O²⁻ dominant at the *W* site” compositions. The compositions of the three samples overlap in terms of *X*-site vacancy, with ranges of values of 0.49–0.80, 0.66–0.82, and 0.61–0.87. However, the three samples are distinct with respect to Fe/(Fe + Mg), which varies from 0.904 to 0.941 in Sample 1, varies widely from 0.347 to 0.876 in Sample 2, and is tightly constrained between 0.980 and 0.999 in Sample 3 (Table 2, Fig. 4A). Most of the tourmaline data fall within the foitite field, with the exception of the cores of Sample 2, which are best classified as magnesiofoitite, where the Fe/(Fe + Mg) value ranges from 0.3 to 0.5. By comparison with available compositions of alkali-deficient tourmaline from other localities and different geological settings (Fig. 4B), it is apparent that tourmaline in the Baraboo quartz veins represents the most strongly alkali-deficient variety recorded to date.

To evaluate the controlling substitutions in the tourmaline, a series of binary composition diagrams are employed, and the arrays of data are compared to reference exchange-vectors that represent hypothetical schemes of substitution (Table 3). In a plot of Fe versus Mg (Fig. 5), tourmaline data from samples 1 and 3 exhibit a distribution roughly parallel to the FeAl₁ and □Al(NaFe)₁ exchange vectors. For Sample 2, the only one containing appreciable amounts of Mg, a least-squares fit to the approximately linear data array yields the expression $\text{Fe} = -0.895(\text{Mg}) + 2.053$, with a correlation coefficient of -0.98 . Based on a slope of -0.895 , it can be argued that most of the Mg incorporation is explained by a simple homovalent MgFe₁ substitution. However, the minor deviation of the linear fit to the data from a slope of -1 suggests that other substitutions, such as □Al(NaMg)₁, □Al(NaFe)₁ and FeAl₁, contribute to the dispersion of the data, and likely result in a deviation from a slope of -1 . If MgFe₁ is the predominant mechanism of substitution, this vector may be used to project to an Mg-free system simply by adding Mg to

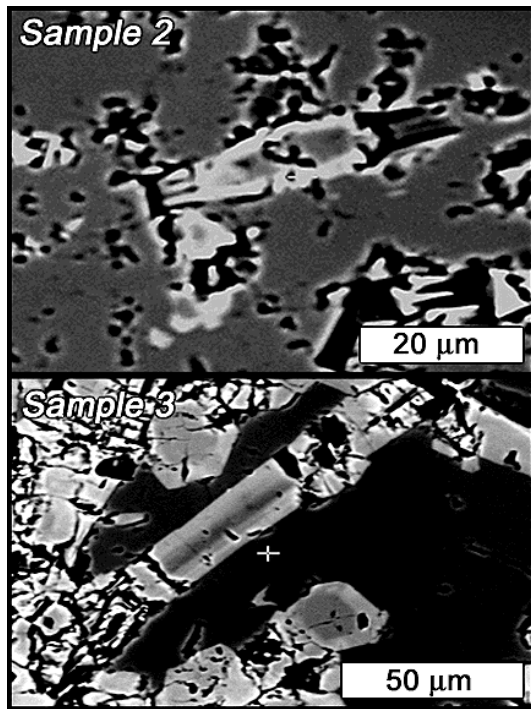


FIG. 2. Back-scattered electron images of compositionally zoned tourmaline in Samples 2 and 3. Grains cut approximately parallel and perpendicular to the *c* axis are shown for each sample.

TABLE 2. REPRESENTATIVE COMPOSITIONS OF ALKALI-DEFICIENT TOURMALINE FROM QUARTZ VEINS IN THE BARABOO QUARTZITE

	Sample 1 (vein in paleosol)				Sample 2 (vein in Baxter Hollow)					Sample 3 (vein in Pine Hollow)						
	max Na	min Na	mean n = 12	1 σ	max Na	min Na	max Mg	min Mg	mean n = 12	1 σ	max Na	min Na	max Al	min Al	mean n = 32	1 σ
wt%																
SiO ₂	35.09	35.14	35.00	0.51	35.83	35.23	36.97	35.03	35.85	0.58	35.29	35.50	34.84	35.29	0.46	
Al ₂ O ₃	31.49	34.00	32.91	0.94	35.29	35.05	34.25	34.36	34.74	0.48	33.73	39.09	30.99	35.00	1.97	
FeO	15.63	13.98	14.96	0.80	10.91	12.35	5.74	13.14	10.79	2.34	16.82	9.08	17.17	13.77	2.09	
MgO	0.93	0.49	0.64	0.14	2.33	1.11	6.07	1.04	1.90	1.51	0.02	0.10	0.01	0.01	0.07	
Na ₂ O	1.51	0.62	0.92	0.28	1.05	0.55	0.82	0.61	0.77	0.15	1.20	0.41	1.05	0.75	0.22	
Sum	84.66	84.23	84.43		85.41	84.29	83.86	84.18	84.05		87.06	84.18	84.06	84.81		
cations based on 15 T+Z+Y																
Si	6.07	6.01	6.02	0.05	5.97	5.97	6.08	5.97	6.07	0.05	5.94	5.96	6.10	6.01	0.05	
Al	6.42	6.86	6.67	0.16	6.93	7.00	6.64	6.90	6.93	0.10	6.69	7.74	6.39	7.03	0.32	
Fe	2.26	2.00	2.15	0.12	1.52	1.75	0.79	1.87	1.53	0.34	2.37	1.28	2.51	1.96	0.32	
Mg	0.24	0.12	0.16	0.04	0.58	0.28	1.49	0.26	0.48	0.37	0.01	0.03	0.00	0.00	0.00	
Na	0.51	0.20	0.31	0.10	0.34	0.18	0.26	0.20	0.25	0.05	0.39	0.13	0.36	0.25	0.08	
charge	49.08	49.09	49.01	0.10	49.21	49.12	49.06	49.03	49.31	0.10	48.96	49.79	48.94	49.29	0.26	
site occupancies based on 15 T+Z+Y																
\square	0.49	0.80	0.69	0.09	0.66	0.82	0.74	0.80	0.75	0.05	0.61	0.87	0.64	0.75	0.08	
X	0.51	0.20	0.31	0.09	0.34	0.18	0.26	0.20	0.25	0.05	0.39	0.13	0.36	0.25	0.08	
Y	2.93	2.99	2.98	0.05	3.03	3.03	2.92	3.03	2.93	0.05	3.06	3.04	2.90	2.99	0.04	
T(Si)*	6.07	6.01	6.02	0.05	5.97	5.97	6.08	5.97	6.07	0.05	5.94	5.96	6.10	6.01	0.04	
Fe/(Fe+Mg)	0.904	0.941	0.929	0.014	0.724	0.861	0.347	0.876	0.761	0.164	0.998	0.980	0.999	0.999	0.010	

* Where $T(\text{Si}) < 6.00$, it is likely that small amounts of Al occur at the T site

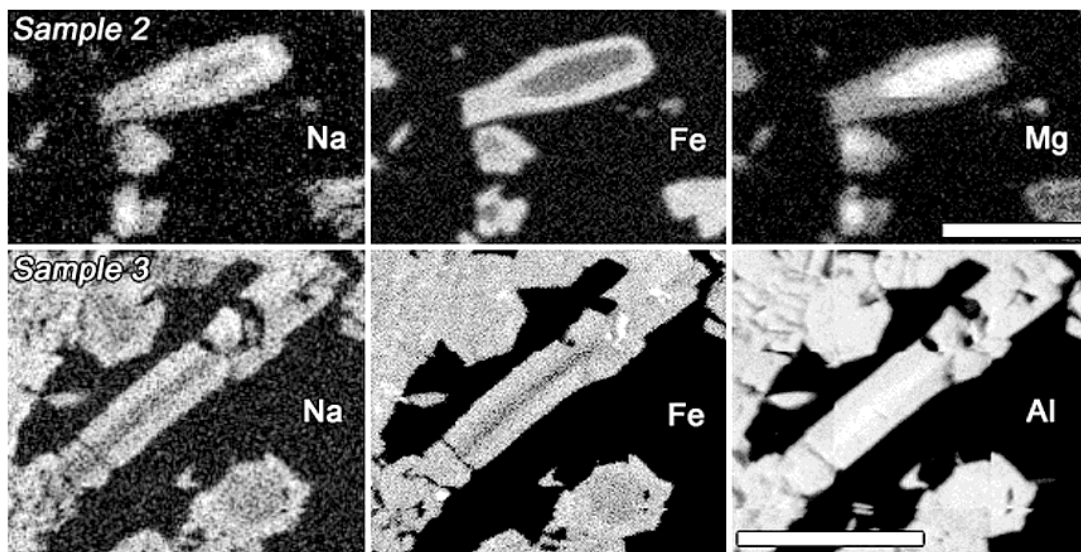


FIG. 3. Element-distribution maps for selected elements in tourmaline in samples 2 and 3 (these are the same grains that appear in Figure 2). Brighter tones represent higher elemental concentrations. Scale bar is 20 μm for sample 2 and 50 μm for sample 3.

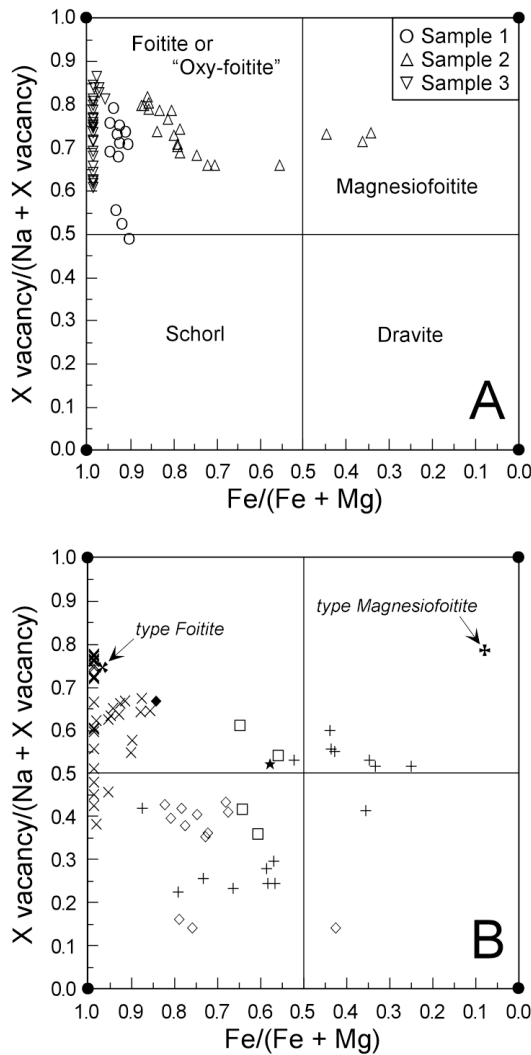


FIG. 4. A) Compositions of Baraboo tourmaline plotted in terms of X vacancy and Fe/(Fe + Mg). End-member compositions of foitite, "oxy-foitite", magnesiofoitite, schorl, and dravite plot at the corners of the diagram. B) Compositions of alkali-deficient tourmaline reported in the literature. Symbols designate various modes of occurrence: bold cross: type foitite, pegmatite (MacDonald *et al.* 1993), crosses: pegmatites (Aurisicchio *et al.* 1999, Dutrow & Henry 2000, Novák & Taylor 2000, Pezzotta *et al.* 1996, Selway *et al.* 1999, 2000), bold plus sign: type magnesiofoitite, hydrothermally altered volcanic rock (Hawthorne *et al.* 1999), plus signs: hydrothermally altered volcanic and sedimentary rocks (Foit *et al.* 1989, Jiang *et al.* 1997, Pesquera *et al.* 1999), filled diamond: quartz vein in Ortega Quartzite (Francis *et al.* 1999), open diamonds: quartz veins in monzonite and syenite (Yavuz *et al.* 1999), open squares: quartz vein in the Tauern Window (Henry *et al.* 2002), star: metakarstbauxite (Henry & Dutrow 2001).

Fe. The value R is used to denote the sum of Mg and Fe, *i.e.*, the vector projection associated with MgFe_{-1} . We recognize that some of Fe is likely to be Fe^{3+} ; the attendant consequences will be examined further.

The R (Fe+Mg) versus Al diagram (Fig. 6A) illustrates the very large range of Al and R, from almost schorl through foitite to "oxy-foitite" (Fig. 6A). A least-squares fit of these data produces a well-constrained line, $R = -0.938(\text{Al}) + 8.568$, with a correlation coefficient of -0.99 . The slope of nearly -1 is consistent with Al variation being due to any or all of the following exchange vectors: $\square\text{Al}(\text{NaR})_{-1}$, $\text{AlO}[\text{R}(\text{OH})]_{-1}$ and FeAl_{-1} . However, to estimate the relative contribution of each of these substitutions to the range in Al and R, it is useful to isolate the influence of the $\square\text{Al}(\text{NaR})_{-1}$ exchange.

The X vacancy versus Al diagram (Fig. 6B) permits some separation of the influence of the $\square\text{Al}(\text{NaR})_{-1}$ ex-

TABLE 3. IMPORTANT SITE-SUBSTITUTIONS AND CORRESPONDING EXCHANGE-VECTORS IN TOURMALINE FROM THE BARABOO QUARTZITE

Site substitution*	Exchange vector
${}^1\text{Fe}^{2+} = {}^1\text{Mg}$	MgFe_{-1}
${}^1\text{or } {}^2\text{Al} = {}^1\text{or } {}^2\text{Fe}^{3+}$	FeAl_{-1}
${}^2\text{Na} + {}^1\text{or } {}^2\text{Mg} = {}^2\text{Al}$	$\square\text{Al}(\text{NaMg})_{-1}$
${}^2\text{Na} + {}^1\text{Fe}^{3+} = {}^2\text{Al}$	$\square\text{Al}(\text{NaFe})_{-1}$
${}^2\text{Na} + {}^1\text{or } {}^2\text{R}^{**} = {}^2\text{Al}$	$\square\text{Al}(\text{NaR})_{-1}$
${}^1\text{or } {}^2\text{R} + {}^1\text{OH} = {}^1\text{or } {}^2\text{Al} + {}^1\text{O}^2$	$\text{AlO}[\text{R}(\text{OH})]_{-1}$

* Precursor superscripts designate specific sites in tourmaline.

** R represents the sum of Fe + Mg.

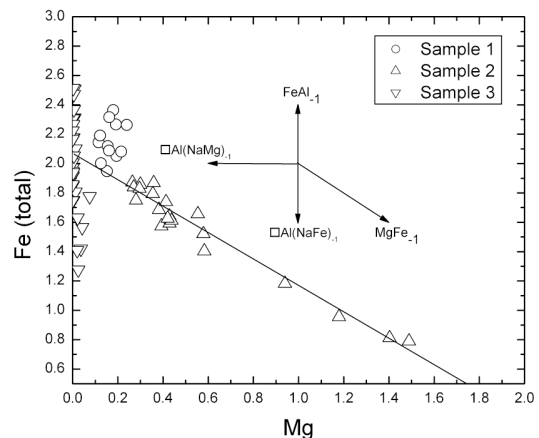


FIG. 5. Fe (total) versus Mg diagram for tourmaline data from all samples. The solid line represents a linear least-squares regression through the data for Sample 2. The directions of several selected exchange-vectors are shown for reference.

change from those of the $\text{AlO}[\text{R}(\text{OH})]_{-1}$ and FeAl_{-1} exchanges on the range of Al and R. If Al is incorporated into tourmaline exclusively *via* the $\square\text{Al}(\text{NaR})_{-1}$ substitution, the slope of the data array in the plot will be +1, but if it is exclusively due to the $\text{AlO}[\text{R}(\text{OH})]_{-1}$ or FeAl_{-1} substitution, or both, the slope of the data array will be 0. The data from all three of the Baraboo samples generally have values for X-site vacancy greater than 0.5, and a least-squares linear fit to the data results in a rather poorly correlated regression expression for X vacancy = $0.195(\text{Al}) - 0.615$, with a correlation coefficient of 0.70. This relatively shallow slope implies that the range of Al associated with chemical zoning is a consequence of roughly 20% substitution of Al *via* the $\square\text{Al}(\text{NaR})_{-1}$ exchange and 80% from that of the $\text{AlO}[\text{R}(\text{OH})]_{-1}$ and FeAl_{-1} exchanges. However, the influence of the $\square\text{Al}(\text{NaR})_{-1}$ substitution remains important, because extrapolation of the least-squares fit to $\text{Al} = 6$ *apfu* still yields a highly alkali-deficient tourmaline. The original local chemical environment must have been Al-rich and Na-poor, resulting in tourmaline that reflects a significant amount of $\square\text{Al}(\text{NaR})_{-1}$ exchange (*e.g.*, von Goerne *et al.* 2001).

The $(\text{R} [\text{Fe} + \text{Mg}] + \text{X vacancy})$ versus $(\text{Al} - \text{X vacancy})$ diagram (Fig. 7A) strips out the influence of $\square\text{Al}(\text{NaR})_{-1}$ by projecting down this vector to the Al-R compositional plane, yielding a rough indication of the relative importance of $\text{AlO}[\text{R}(\text{OH})]_{-1}$ and FeAl_{-1} , and condensing the compositions of schorl and foitite to a common point. A linear least-squares fit to the transformed data has a slope close to -1, $(\text{Fe} + \text{Mg} + \text{X}$

vacancy) = $-0.932(\text{Al} - \text{X vacancy}) + 8.578$, with a correlation coefficient of -0.98, implying that most of the residual Al variation is due to a combination of the $\text{AlO}[\text{R}(\text{OH})]_{-1}$ and FeAl_{-1} exchanges. However, it is possible to establish the relative importance of each substitution. Those data points that plot to the left of the schorl-foitite point will represent a minimum contribution of the FeAl_{-1} exchange (up to roughly 0.2 *apfu*), and those data to the right of the schorl-foitite point will represent a minimum contribution of the $\text{AlO}[\text{R}(\text{OH})]_{-1}$ exchange (0-0.9 *apfu*). These are minimal contributions because they react to offset calculation effects (Henry & Dutrow 1996). Nonetheless, it is unlikely that the $\text{AlO}[\text{R}(\text{OH})]_{-1}$ vector will extend beyond the "oxy-foitite" composition, so this will serve as a reasonable minimum estimate of the amount of deprotonation in the tourmaline, *i.e.*, O^{2-} for OH^- at the W site. Of particular note is that five compositions of the core of Sample 3 tourmaline fall closer to the "oxy-foitite" end-member composition than the foitite-schorl point, and can be most reasonably classified as "oxy-foitite", although H_2O has not been determined directly.

The (excess charge) versus $(\text{R}[\text{Fe} + \text{Mg}] + \text{X vacancy})$ diagram (Fig. 7B) serves as a rough approximation of the amount of Fe as Fe^{3+} and the amount of deprotonation. Because these two factors have offsetting effects on charge calculation, the calculated values of excess charge represent minima. However, a number of compositions have a charge deficiency (<0), which indicates that some Fe^{3+} is present in portions of the tourmaline. The presence of Fe^{3+} is also indicated by

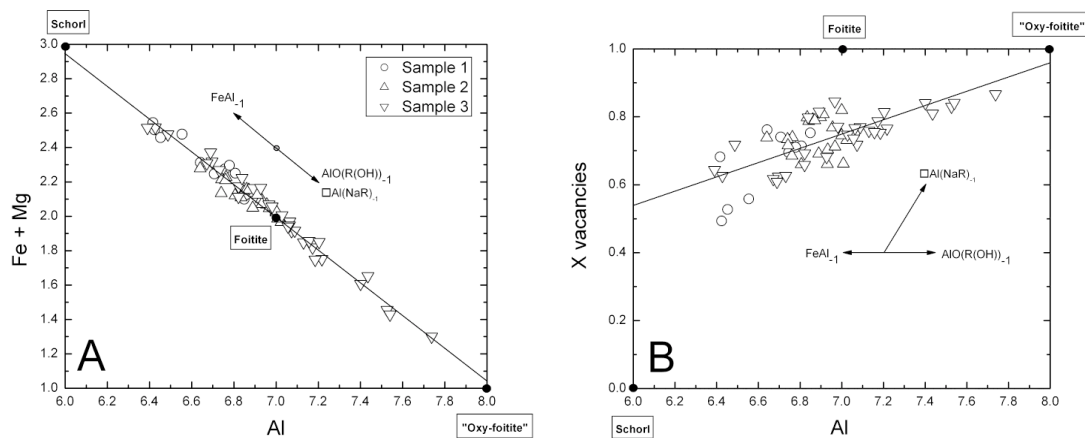


FIG. 6. A) $\text{R}(\text{Fe} + \text{Mg})$ versus Al diagram for tourmaline data from all samples. R represents the sum of $\text{Fe}(\text{total}) + \text{Mg}$, *i.e.*, the condensation of the data down the FeMg_{-1} vector. The solid line represents a linear least-squares regression through the data from all samples. The directions of several selected exchange-vectors are shown for reference. The locations of end-member schorl, foitite and "oxy-foitite" are designated by the filled circles. B) Diagram showing Al versus X vacancy for tourmaline data from all samples. The solid line represents a linear least-squares regression through the data from all samples. The directions of several selected exchange-vectors are shown for reference. The location of the end-member schorl, foitite and "oxy-foitite" are designated by the filled circles.

the intense pleochroism of the Baraboo tourmaline, which reflects the interaction of Fe^{3+} with Fe^{2+} . The tourmaline data in Figure 7B have a linear least-squares fit with a negative slope of ~ 1 : (excess charge) = $-0.974(\text{Fe} + \text{Mg} + \text{X vacancy}) + 2.931$, with a correlation coefficient of -0.98 . The relatively high excess charge for many compositions is further evidence for deprotonation at the *W* site, and several of the core compositions in Sample 3 extend very close to the hypothetical “oxy-foitite” end-member. It should be noted that the Baraboo tourmaline coexists with hematite, and experiments have demonstrated that tourmaline crystallized at high levels of $f(\text{O}_2)$ can have a relatively high ratio of Fe^{3+} to total Fe (Fuchs *et al.* 1998). A complete chemical characterization of the Baraboo tourmaline requires independent measurements of Fe^{3+} and OH; thus, the calculated cation charges and estimated oxy-foitite contents given here may not be entirely accurate. Nevertheless, the high Al contents and the high calculated excess charges for the cores of tourmaline grains in Sample 3 require a substantial “oxy-foitite” component, on the order of 70 to 80 mol.%.

DISCUSSION

Foitite from other occurrences differs from that at Baraboo in containing appreciable quantities of Ti, Mn, Ca, Li and F, depending on locality, and in being associated with a variety of silicate minerals, including al-

bite, “adularia”, micas and zeolites, among others. In contrast, the Baraboo foitite is chemically simple, containing only Si, Al, Fe, Mg, and Na (+ B + O + H), and is accompanied solely by quartz and hematite.

Compositions of alkali-deficient tourmaline reported in the literature span the same range of Fe/(Fe + Mg) as that for the Baraboo tourmaline, but typically display a higher occupancy of the *X* site (Fig. 4B), with many samples having less than 50% vacancy, thus being Na-poor schorl and dravite, rather than true foitite. Among the various occurrences of alkali-deficient tourmaline, those from pegmatites have the highest *X*-site vacancies, comparable to those in the Baraboo tourmaline, although such tourmaline typically may contain significant amounts of Li.

In terms of geological occurrence, foitite from Copper Mountain, New Mexico (Francis *et al.* 1999) is most comparable to that at Baraboo. The Copper Mountain foitite occurs in a quartz vein that cuts the Ortega Quartzite, which is considered to be correlative with the Baraboo Quartzite (Medaris *et al.* 2003). With respect to mineral assemblage, the Copper Mountain foitite is associated with scheelite and “wolframite”, rather than hematite, and crystallized at relatively low oxygen fugacity, below that of the quartz – fayalite – iron buffer. The Copper Mountain foitite is compositionally similar to foitite in Baraboo Samples 1 and 2 (*cf.* Figs. 4A, B),

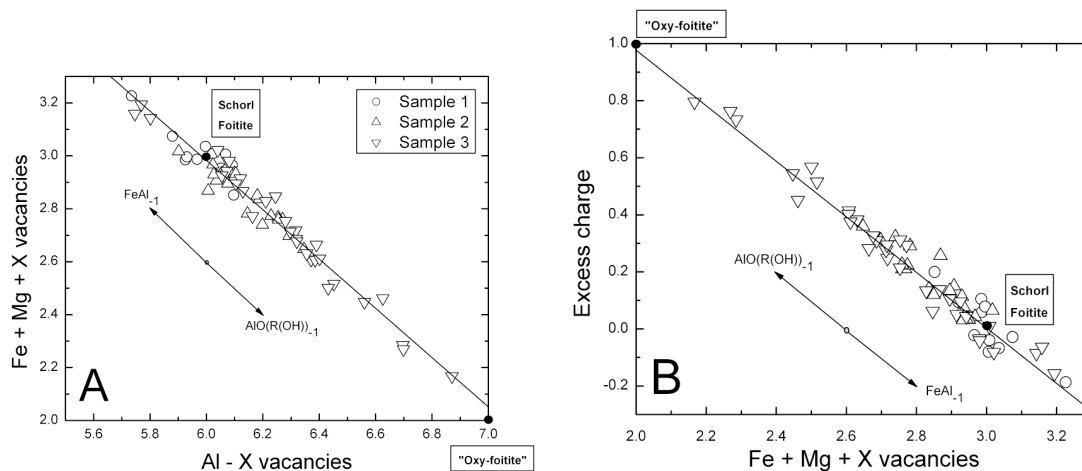


FIG. 7. A) Diagram showing (R + X vacancies) versus (Al – X vacancies) for tourmaline data from all samples. R represents the sum of Fe(total) + Mg, *i.e.*, the condensation of the data down the FeMg_{-1} vector. The (Al – X vacancies) and (R + X vacancies) terms result in the condensation of the data down the $\square\text{Al}(\text{NaR})_{-1}$ exchange-vector. The solid line represents a linear least-squares regression through the data from all samples. The directions of several selected exchange-vectors are shown for reference. The locations of end-member schorl, foitite and “oxy-foitite” are designated by the filled circles. B) Diagram showing (excess charge) versus (R + X vacancies) for tourmaline data from all samples. The excess charge is the sum of the total cation charge that is in excess of a total charge of 58, assuming all Fe as Fe^{2+} (*cf.* Henry & Dutrow 1996). The solid line represents a linear least-squares regression through the data from all samples. The directions of several selected exchange-vectors are shown for reference. The locations of end-member schorl, foitite and “oxy-foitite” are designated by the filled circles.

except for the presence of small amounts of Ti (0.35 wt% TiO₂) and F (0.20 wt%). The major compositional distinction in tourmaline from the two localities is the high aluminum content and presence of substantial "oxy-foitite" component in the cores of tourmaline grains in Baraboo Sample 3.

The composition of the Baraboo tourmaline reflects in large part its environment of formation within the chemically mature Baraboo metasedimentary rocks. However, the zoning characteristics of the tourmaline are the result of chemical changes in the hydrothermal fluids associated with quartz vein formation. During post-Penokean folding and low-grade metamorphism at 1.63 Ga, hydrothermal fluids migrated through the alkali-depleted Baraboo sequence, where they scavenged B and the other elements necessary to precipitate quartz, hematite, and foitite. The exceptionally mature Baraboo Quartzite, which consists almost entirely of SiO₂, Al₂O₃, Fe₂O₃, and H₂O, is the product of Proterozoic weathering and sedimentation (Medaris *et al.* 2003), and the chemical and mineralogical compositions of quartz veins in the quartzite are largely inherited from such processes. However, the core-to-rim compositional variation in the Baraboo tourmaline demonstrates that an evolving hydrothermal fluid was also an important factor influencing tourmaline composition. From a qualitative comparison with experimental results on the distribution of Na between tourmaline and fluid (von Goerne *et al.* 2001), the composition of the hydrothermal fluid is considered to have evolved from an initial Na-poor and relatively alkaline condition to one that was richer in Na and more acidic (*cf.* Henry *et al.* 2002). In the case of the magnesiofoitite cores in Sample 2, Mg was likely to be locally derived in the early stage of tourmaline growth. In general, the core-to-rim compositional changes in the Baraboo tourmaline may have resulted from the predominant, buffering influence of the host quartzite in the early stage of quartz vein formation and the increasingly important role of hydrothermal fluids as the system matured.

ACKNOWLEDGEMENTS

We thank Bruce Brown for providing access to the Baxter Hollow drill core, from which Sample 1 was obtained, and Paul Herr for contributing Sample 3. The Weeks Bequest of the Department of Geology and Geophysics provided funds for the electron-microprobe analyses and the acquisition of the images. We thank George Rossman and Andreas Ertl for their constructive reviews, and Franklin F. Foit, Jr., for editorial handling of the manuscript.

REFERENCES

- ARMSTRONG, J.T. (1988): Quantitative analysis of silicate and oxide materials: comparison of Monte Carlo, ZAF, and $\phi(\rho z)$ procedures. *In* Microbeam Analyses (D.E. Newbury, ed.). San Francisco Press, San Francisco, California (239-246).
- AURISICCHIO, C., OTTOLINI, L. & PEZZOTTA, F. (1999): Electron- and ion-microprobe analyses, and genetic inferences of tourmalines of the foitite-schorl solid solution, Elba Island (Italy). *Eur. J. Mineral.* **11**, 217-225.
- DUTROW, B.L. & HENRY, D.J. (2000): Complexly zoned fibrous tourmaline, Cruzeiro mine, Minas Gerais, Brazil: a record of evolving magmatic and hydrothermal fluids. *Can. Mineral.* **38**, 131-143.
- FOIT, F.F., JR., FUCHS, Y. & MYERS, P.E. (1989): Chemistry of alkali-deficient schorls from two tourmaline-dumortierite deposits. *Am. Mineral.* **74**, 1317-1324.
- FRANCIS, C.A., DYAR, M.D., WILLIAMS, M.L. & HUGHES, J.M. (1999): The occurrence and crystal structure of foitite from a tungsten-bearing vein at Copper Mountain, Taos County, New Mexico. *Can. Mineral.* **37**, 1431-1438.
- FUCHS, Y., LAGACHE, M. & LINARES, J. (1998): Fe-tourmaline synthesis under different T and f(O₂) conditions. *Am. Mineral.* **83**, 525-534.
- HAWTHORNE, F.C. & HENRY, D.J. (1999) Classification of the minerals of the tourmaline group. *Eur. J. Mineral.* **11**, 201-215.
- _____, SELWAY, J.B., KATO, A., MATSUBARA, S., SHIMIZU, M., GRICE, J.D. & VAJDAK, J. (1999): Magnesiofoitite, $\square(\text{Mg}_2\text{Al})\text{Al}_6(\text{Si}_6\text{O}_{18})(\text{BO}_3)_3(\text{OH})_4$, a new alkali-deficient tourmaline. *Can. Mineral.* **37**, 1439-1443.
- HENRY, D.J. & DUTROW, B.L. (1996): Metamorphic tourmaline and its petrologic applications. *In* Boron: Mineralogy, Petrology and Geochemistry (E.S. Grew & L.M. Anovitz, eds.). *Rev. Mineralogy* **33**, 503-557.
- _____, _____ (2001): Compositional zoning and element partitioning in nickeloan tourmaline from a metamorphosed karstbauxite from Samos, Greece. *Am. Mineral.* **86**, 1130-1142.
- _____, _____ & SILVERSTONE, J. (2002): Compositional asymmetry in replacement tourmaline – an example from the Tauern Window, Eastern Alps. *Geol. Mater. Res.* **4**, 1-18.
- JIANG, SHAO-YONG, PALMER, M.R. & SLACK, J.F. (1997): Alkali-deficient tourmaline from the Sullivan Pb-Zn-Ag deposit, British Columbia. *Mineral. Mag.* **61**, 853-860.
- MACDONALD, D.J., HAWTHORNE, F.C. & GRICE, J.D. (1993): Foitite, $\square[\text{Fe}^{2+}_2\text{Al,Fe}^{3+}]\text{Al}_6\text{Si}_6\text{O}_{18}(\text{BO}_3)_3(\text{OH})_4$, a new alkali-deficient tourmaline: description and crystal structure. *Am. Mineral.* **78**, 1299-1303.
- MEDARIS, L.G., JR. & FOURNELLE, J.H. (2000): Tourmaline-bearing quartz veins in the Baraboo Quartzite: a new occurrence of the alkali-deficient tourmaline, foitite. *46th Int. Lake Superior Geol., Proc. Abstr.* **46**, 39-40.

- _____, SINGER, B.S., DOTT, R.H., JR., NAYMARK, A., JOHNSON, C.M. & SCHOTT, R.C. (2003) Late Paleoproterozoic climate, tectonics and metamorphism in the southern Lake Superior region and proto-North America: evidence from Baraboo interval quartzites. *J. Geol.* **111**, 243-257.
- NOVÁK, M. & TAYLOR, M.C. (2000): Foitite: formation during late stages of evolution of complex granitic pegmatites at Dobrá Voda, Czech Republic, and Pala, California, U.S.A. *Can. Mineral.* **38**, 1399-1408.
- PESQUERA, A., TORRES-RUIZ, J., GIL-CRESPO, P.P. & VELILLA, N. (1999): Chemistry and genetic implications of tourmaline and Li-F-Cs micas from the Valdeflores area (Cáceres, Spain). *Am. Mineral.* **84**, 55-69.
- PEZZOTTA, F., HAWTHORNE, F.C., COOPER, M.A. & TEERTSTRA, D.K. (1996): Fibrous foitite from San Piero in Campo, Elba, Italy. *Can. Mineral.* **34**, 741-744.
- SELWAY, J.B., ČERNÝ, P., HAWTHORNE, F.C. & NOVÁK, M. (2000): The Tanco pegmatite at Bernic Lake, Manitoba. XIV. Internal tourmaline. *Can. Mineral.* **38**, 877-891.
- _____, NOVÁK, M., ČERNÝ, P. & HAWTHORNE, F.C. (1999): Compositional evolution of tourmaline in lepidolite-subtype pegmatites. *Eur. J. Mineral.* **11**, 569-584.
- VON GOERNE, G., FRANZ, G. & HEINRICH, W. (2001): Synthesis of tourmaline solid solutions in the system Na₂O-MgO-Al₂O₃-SiO₂-B₂O₃-H₂O-HCl and the distribution of Na between tourmaline and fluid at 300 to 700°C and 200 MPa. *Contrib. Mineral. Petrol.* **141**, 160-173.
- YAVUZ, F., ÇELİK, M. & KARAKAYA, N. (1999): Fibrous foitite from Sebinkarahisar, Giresun Pb-Zn-Cu-(U) mineralized area, northern Turkey. *Can. Mineral.* **37**, 155-161.

Received January 25, 2003, revised manuscript accepted April 12, 2003.